HHS Public Access

Author manuscript

Biosens Bioelectron X. Author manuscript; available in PMC 2023 December 20.

Published in final edited form as:

Biosens Bioelectron X. 2023 December ; 15: . doi:10.1016/j.biosx.2023.100402.

Development of integrated smartphone/resistive biosensor for on-site rapid environmental monitoring of organophosphate pesticides in food and water

Hussian Maanaki[a,b], **Terry Xu**[c], **Guibing Chen**[d], **Xiuxia Du**[a,e], **Jun Wang**[a,b,e,*]

[a]Department of Bioinformatics and Genomics, University of North Carolina at Charlotte, Charlotte, NC, 28223, USA

[b]NanoDiagnostic Technology, LLC, Kannapolis, NC, 28081, USA

[c]Department of Mechanical Engineering, University of North Carolina at Charlotte, Charlotte, NC, 28223, USA

[d]Center for Excellent in Post-Harvest Technologies, North Carolina A & T State University, NC Research Campus, Kannapolis, NC, 28081, USA

[e]Center for Environmental Monitoring and Informatics Technologies for Public Health, University of North Carolina at Charlotte, Charlotte, NC, 28223, USA

Abstract

Organophosphate (OP) pesticides remain a worldwide health concern due to their acute or chronic poisoning and widespread use in agriculture around the world. There is a need for robust and field-deployable tools for onsite detection of OP pesticides in food and water. Herein, we present an integrated smartphone/resistive biosensor for simple, rapid, reagentless, and sensitive monitoring of OP pesticides in food and environmental water. The biosensor leverages the hydrolytic activity of acetylcholinesterase (AChE) to its substrate, acetylcholine (ACh), and unique transport properties of polyaniline nanofibers (PAnNFs) of chitosan/AChE/PAnNF/carbon nanotube (CNT) nanocomposite film on a gold interdigitated electrode. The principle of the sensor relies on OP inhibiting AChE, thus, reducing the rate of ACh hydrolysis and consequently decreasing the rate of protons doping the PAnNFs. Such resulted decrease in conductance of PAnNF can be used to quantify OP pesticides in a sample. A mobile app for the biosensor was developed for analyzing measurement data and displaying and sharing testing results. Under optimal conditions, the

*Corresponding author. Department of Bioinformatics and Genomics, University of North Carolina at Charlotte, NC, USA. jun.wang@charlotte.edu (J. Wang).

CRediT authorship contribution statement

Hussian Maanaki: Investigation, Methodology, Validation, Data curation, Software, Writing - original draft. **Terry Xu:** Data curation. **Guibing Chen:** Validation, Data curation. **Xiuxia Du:** Formal analysis, Supervision, Software. **Jun Wang:** Conceptualization, Methodology, Funding acquisition, Project administration, Resources, Supervision, Writing – review & editing.

Declaration of competing interest

The authors declare that they have no known competing financial interests or personal relationships that could have appeared to influence the work reported in this paper.

Appendix B. Supplementary data

Supplementary data to this article can be found online at https://doi.org/10.1016/j.biosx.2023.100402.

biosensor demonstrated a wide linear range (1 ppt–100 ppb) with a low detection limit (0.304 ppt) and high reproducibility (RSD <5%) for Paraoxon-Methyl (PM), a model analyte. Furthermore, the biosensor was successfully applied for analyzing PM spiked food/water samples with an average recovery rate of 98.3% and provided comparable results with liquid chromatography-mass spectrometry. As such, the nanosensing platform provides a promising tool for onsite rapid and sensitive detection of OP pesticides in food and environmental water.

Keywords

Resistive nanosensor; Mobile app; Polyaniline nanofibers; Acetylcholinesterase; Organophosphate pesticides

1. Introduction

Organophosphate (OP) pesticides remain as an environmental and health concern worldwide (Karami-Mohajeri and Abdollahi, 2011; Liu and Lin, 2005). These pesticides are the most common toxins in food and water because of their widespread use in the agricultural industry to maintain the health and yield of crops across the world. They are frequently found on the surface of foods and are taken up by plants through contaminated soil and water. Consumption of food and water contaminated with these pesticides results in negative health effects due to their neurotoxicity. OP pesticides are neurotoxicants due to their irreversible inhibition of cholinergic esterases, such as acetylcholinesterase (AChE) and butyrylcholinesterase (BChE). AChE is essential for facilitating the hydrolysis of the neurotransmitter, acetylcholine (ACh), terminating neurotransmission in humans and insects. Inhibitory effects due to OP binding to AChE results in over-accumulation of ACh within the synapse and neuromuscular junction, which causes headaches, blurred vision, muscle twitching, paralysis, respiratory and cardiovascular symptoms, and even death (King and Aaron, 2015). In particular, their effects during prenatal development and on children has shown an increased risk of cognitive/behavioral deficits and the development of neurological disorders (Hertz-Picciotto et al., 2018).

Monitoring pesticide residue in food and water represents a major burden for public health efforts. Chromatography coupled with mass spectroscopy (MS) is a standard method for detecting pesticides (Anna, 2016; Souza Tette et al., 2016). For example, gas chromatography (GC) (Berijani et al., 2006; Rezaee et al., 2006) or high-performance liquid chromatography (HPLC) (Beltran et al., 2000), paired with MS, has been widely used for the detection of pesticide residues in food and water. These analytical techniques, although highly sensitive and reliable, have several disadvantages, including complex sample preparation protocols and high cost of operation and maintenance. Furthermore, these methods are time-consuming, require centralized laboratories, and trained personnel and are unsuitable for on-site pesticide detection.

To reduce the health risk and mitigate the adverse health effects, there is a need for sensitive and robust analytical tools for onsite monitoring of pesticides in food and water. Over the last few decades, various biosensors have been developed for the detection of pesticide residues in food and water (Gai et al., 2023; Li et al., 2023; Zhu et al., 2022).

These biosensors fall into two categories: (i) enzyme-based biosensors in tandem with electrochemical and optical techniques (Kaur and Singh, 2020; Loguercio et al., 2021). The sensing principle of these biosensors is based on the enzyme (e.g., cholinesterase) inhibition by pesticides or hydrolysis of pesticides by some enzymes (e.g., organophosphorus hydrolase (OPH)) (Pundir and Chauhan, 2012). (ii) Affinity-based immunosensors with electrochemical and optical techniques (Martini et al., 2015; Zou et al., 2010). During the past few decades, a large number of enzyme-based biosensors with varying detection techniques such as amperometry (Wang et al., 2008; Yu et al., 2015), voltammetry (Thakkar et al., 2019; Yu et al., 2022), potentiometry (Dzyadevych et al., 2004; Ghindilis et al., 1996), conductometry (Arkhypova et al., 2001; Dzyadevych et al., 2005)), colorimetry (Liang and Han, 2020), and fluorescence (Ozturk et al., 2007; Zhang et al., 2012) have been developed for detecting pesticides in food and water. However, few have reached the market for real world applications due to their overall poor performance in: (i) sensitivity, (ii) stability, (iii) simplicity and portability, (iv) cost, or (v) data sharing.

To address these issues, we report on the development of a reagentless, low-cost, and portable enzymatic resistive biosensor integrated with a smartphone mobile app for on-site rapid, quantitative, and sensitive monitoring of OP-pesticides in food and water. To our knowledge, this is the first application of a resistive-based biosensor for detection of OP pesticides through changes in local pH, taking advantage of AChE facilitated hydrolysis of ACh. The system utilizes disposable/recyclable thin-film gold interdigitated electrodes (AuIDEs) that allows for a large transductive surface area while minimizing gap length between the finger electrodes, thus improving sensitivity and detection limits. Furthermore, the modification of AuIDE with a carbon nanotube/polyaniline nanofiber (CNT/PAnNF) film acts as a signal amplifier, allowing for fast response times, improved stability, and high sensitivity for pesticide analysis. The application of PAnNFs as the transducing element is essential, due to its tunable transport properties through changes in doping/dedoping state as a function of pH (Huang et al., 1986; Virji et al., 2004). Moreover, to improve the portability and simplicity of the biosensor, sensing components, such as the ACh substrate, sample pH adjustments, and anti-interference reagents, are pre-dried on a glass fiber (GF) pad for pesticide analysis in a wide-range of food/water samples. Finally, the biosensor is connected to a portable digital multimeter for wireless data transmission to a smartphone with app to record, analyze, display, manage, track, and share pesticide measurement data.

2. Materials and methods

2.1. Materials and other related information

The readers are referred to Supplementary Materials (S) for details: S1 for chemicals and materials, S2 for instrumentation, S3 for synthesis of CNT/PAnNF nanomaterials, and S4 for preparing pesticide spiked food (e.g., orange juice, grape juice, milk, and meat) and water (river and well) samples. Here, we present our sensor design and fabrication, app development, and the methodology for carrying out pesticide measurements in food and water.

2.2. Design and fabrication of chitosan/AChE/CNT/PAnNF-modified AuIDE nanosensor

The nanosensor consists of 3 major components: AuIDE, nanocomposite film on an AuIDE containing a layer of AChE/PAnNF/CNT underneath and a layer of chitosan atop, a pre-treatment pad, i.e., a pre-loaded GF pad (2.5 mm in diameter) with anti-inference reagents, e. g., Ethylenediaminetetraacetic acid (EDTA), and a signal generation pad, i. e., a pre-loaded GF pad (2.5 mm in diameter) with the substrate ACh. The preparation of the nanosensor is illustrated in Fig. S5. First, an AuIDE with 20 μm features were cleaned under light sonication in acetone followed by rinsing with ultrapure deionized (DI) water for 15 min each and subsequently dried under vacuum (Fig. S5 a). To confine the sensing area, a Parafilm template with a hole of 2.5 mm in diameter, made by a biopsy punch, was tightly attached to the sensor surface (Fig. S5 b). After template attachment, the exposed sensing surface was placed with 10 μL of 0.002% Tween-20 for 15 min, and then was rinsed with DI water for 1 min and dried in a vacuum desiccator overnight. Next, partially-dedoped CNT/PAnNF suspension was lightly sonicated for 1 min, and then 4 μL of the CNT/PAnNF suspension was drop-casted onto the exposed sensor surface and allowed to air-dry (Fig. S5 c and d). Following that, 2 μL of AChE in solution was placed on the CNT/PAnNF nanocomposite, where enzymes enter the nanonetwork and are trapped inside. To prevent enzyme from leakage, 2 μL chitosan was dropped onto the enzyme-entrapped nanocomposite and allowed to air-dry in a desiccator at 4 °C (Fig. S5 e). Finally, the parafilm template on the sensor was peeled off and a Chitosan/AChE/PAnNF/CNT nanocomposite-coated nanosensor was prepared (Fig. S5 f) and then stored in a desiccator at 4 °C before use.

To prepare a signal generation pad, a GF membrane was cut into a circle with diameter of 2.5 mm using a biopsy punch, and then the circle pad was loaded with the desired volume of ACh using a pipette. Finally, the ACh-loaded pad was dried and stored in a vacuum desiccator at room temperature before use. It is similar to prepare a pre-treatment pad. Instead of ACh, EDTA and a pH adjustment solution were dispensed onto a circle GF pad with 2.5 mm diameter, and then this reagent-loaded pad was dried and stored in a vacuum desiccator at room temperature. Reagents in a dry state in a pad are much more stable than they are in solution. Thus, these pre-loaded pads provide a possibility for long-term storage of reagents. More importantly, it will allow convenient operations and avoid solution handling for onsite testing.

2.3. Mobile app for data processing and display

A mobile app for the sensing platform was developed in Android Studio using JAVA. Resistive data processing techniques were implemented into the app for automatic data processing, such as: data preprocessing (curve cleaning), peak recognition (maximum resistance), data normalization, signal alignment, inhibition calculations, result display, and data storage, sharing, and management.

2.4. Sample testing protocol

The exact device setup consists of a nanosensor (Fig. S6 A-a) connected to a Bluetooth multimeter (Fig.S6 A-b) and a smartphone with mobile app (Fig. S6 A-c and B). Protocol for measuring OP pesticides in a sample using the developed nanosensor has two steps: 1)

determine baseline AChE activity of a biosensor serving as a control. Briefly, generation of a control signal begins by applying 15 μL DI water on the surface of a nanosensor with initial resistance of ~20 MΩ and then adding a signal generation pad in the water. ACh quickly dissolves in the water and diffuses into the nanocomposite where the enzymatic reaction takes place, generating a response of resistance change over time. Following the generation of the control signal, the reaction solution and GF pad on the nanosensor are removed; 2) determine remaining AChE activity after the incubation with a sample. To achieve this, 15 μL of the sample is placed on the nanosensor surface along with a pre-treatment pad and incubated for 10 min to allow for OP pesticide binding to AChE. Once the incubation period finishes, the sample solution is removed from the sensor surface. Subsequently, 15 μL of water is added onto it with initial resistance of ~20 MΩ in the same manner as the control. Then, a signal generation pad is added to the water to generate the response, which would be smaller due to AChE inhibition by OP from the sample. After finishing the control test and sample test, the raw measurement data in CSV format from two tests are analyzed by the app (described in section 2.3 and 3.2). Thereafter, the results of both enzyme inhibition and pesticide concentration in the sample are determined and displayed on the screen of the smartphone (Fig. S6 B).

3. Results and discussion

3.1. Analytical principle of the resistive biosensor

In this study, the principle of the nanosensor is based on AChE inhibition by OP pesticides and the unique transport properties of PAnNFs. The functioning of the system relies on the enzymatic reaction between AChE and ACh (Fig. 1A). AChE hydrolyzes ACh into choline and acetic acid (CH_3COOH), at the rate of 25,000 ACh per second. The latter dissociates into an acid residue and a proton (Fig. 1A). The generation and local accumulation of protons results in rapid doping of the PAnNFs, which causes a conductance change across the AuIDE (Fig. 1D – black line). This conductance change over time is recorded by a digital meter with Bluetooth (Fig. 1C) and transmitted to a smartphone with app (Fig. 1D). Addition of a sample containing pesticides to a sensor surface results in inhibition of AChE by OP (Fig. 1B), thus reducing the proton generation and consequently reducing conductance changes and even no conductance changes if enzyme is fully inhibited by OP pesticides (Fig. 1D – red line). As a result, the change in conductance is directly proportional to the enzymatic activity at the sensing surface. Through OP inhibitory effects on AChE, the change in conductance becomes inversely proportional to the concentration of pesticide residue within a sample. Thus, this method can be used to quantitatively measure the concentration of pesticides in a sample. The enzyme inhibition by pesticides can be calculated according to the following equations:

$$\text{AChE Inhibition} = \frac{(\text{Rs}_{\text{initial}} - \text{Rs}_{\text{sample}})}{\text{Rs}_{\text{initial}}} * 100\,\% \quad (1)$$

$$\text{Rs}_{\text{initial}}, \text{Rs}_{\text{sample}} = \left(\frac{\text{R}}{\text{R}_{\text{initial}}}\right)^{-1} \quad (2)$$

Here, $Rs_{initial}$ represents the original enzyme activity measured from a nanosensor without any pesticides, which serves as a control. Rs_{sample} is for depressed enzyme activity from the nanosensor exposed to pesticides in a sample. $Rs_{initial}$ and Rs_{sample} are reciprocal of normalized resistance change R of a nanosensor for control and sample, respectively. The normalization of measured resistance R is obtained by dividing resistance R of a nanosensor by the initial resistance ($R_{initial}$) at the starting point of the enzyme reaction. Once enzyme inhibition (Eqn. (1)) is known, concentration of pesticide in a sample can be determined by using an established calibration curve.

3.2. App capabilities

A mobile app for the nanosensor was developed with multiple functions, as outlined in experimental section 2.3. Here, we demonstrate some capabilities of the app. Fig. S6 B exhibits the results of a control and sample testing response generated by the nanosensor. First, the app normalizes raw data for the control (Fig. S6 B, grey line) and the sample (Fig. S6 B, black line), and aligns these two normalized curves together. Second, it can automatically calculate the enzyme inhibition at each time point from the control data and the sample data according to equation (1), and displays the inhibition curve (Fig. S6 B, red line). Finally, it provides the concentration of pesticide in a sample at the bottom of the screen with error, using the experimentally derived calibration curve.

3.3. Characterization of CNT/PAnNF nanocomposite

Fig. 2A shows the UV–Vis spectra of the CNT/PAnNF nanocomposites in a fully-doped state (0 and 1% wt. CNT, solid and dashed line) and partially-doped state (1% wt. CNT, dotted line). Fully-doped CNT/PAnNF nanocomposites exhibit a wide absorption band between 380 and 420 nm. While such a wide band separates into two distinct peaks at 350 and 430 nm when the nanocomposite is partially-doped (Fig. 2A dotted line). The absorption peaks at 350 and 430 nm correspond to the π-π* transition of benzenoid rings and polaron-π* transition of protonated imines, respectively. As such, the ratio of π-π* to polaron-π* transition can be used to estimate the extent of PAnNF doping (Godovsky et al., 2001). Therefore, the UV–Vis spectra results confirm the presence of conducting emeraldine salt polyaniline in a fully and partially-doped state (Huang et al., 2003; Stejskal et al., 1993). The absorbance (Abs.) intensity at ~350 nm was utilized to determine the concentration of the CNT/PAnNF suspension for tuning the film's thickness prior to drop-casting onto the AuIDE, ensuring the reproducibility of the nanocomposite films (Fig. S8 B). Transmission electron microscopy (TEM) was used to characterize the morphology of the CNT/PAnNF transducing film at wt. 0, 0.25, 1.0, and 2.5% CNT (Fig. 2B and Fig. S7 B). The diameter of the CNT/PAnNF nanocomposites with 0–1.0% wt. CNT was roughly 80 nm, while those synthesized with 2.5% wt. CNT showed an increased thickness, with diameters >100 nm (Fig S7 B-d). TEM images reveal nanofiber features within the CNT/PAnNF nanocomposite.

3.4. Optimization of experimental parameters

Optimization of the resistive biosensor was performed by considering the following factors: CNT content, CNT/PAnNF film thickness, AChE concentration, ACh concentration,

chitosan thickness, sample incubation period, EDTA concentration, and temperature. Since buffers may neutralize protons from the enzymatic reaction and rapidly strip protons from the partially-dedoped PAnNF, causing interference, they should be avoided during testing. Therefore, the optimization of biosensor parameters was performed in DI water.

To improve the stability and reproducibility of PAnNFs, CNTs were used to fabricate hybrid CNT/PAnNF nanocomposite on the nanosensor. The amount of CNT (wt.%: 0, 0.5, 1.0, and 2.5) in CNT/PAnNF suspension were prepared as previously described (S3). Partially-dedoped PAnNFs with varying CNT content were evaluated by assessing the response of the sensor using standard HCl solutions (pH 4–7, Fig. S8 A). It was found that increasing CNT content resulted in a notable decrease in biosensor sensitivity. On the other hand, decreasing presence of CNTs resulted in poor reproducibility, when responses exceeded a 10-fold change. These issues might be attributed to the high conductivity of CNTs, which reduced overall resistance change caused by PAnNF doping. To achieve good sensitivity and reproducibility for the biosensor, optimal CNT content, 1.0%, was selected based on the generation of about 10-fold signal change. Therefore, 1.0% CNT is routinely used throughout this study.

AChE enzyme was immobilized in the CNT/PAnNF nanocomposite on an AuIDE through simple physical entrapment, as an effective and low-cost method (Dwevedi, 2016; Pundir and Chauhan, 2012); though the activity of AChE in nanocomposite could be affected by the slow diffusion of ACh to AChE, due to the barriers around it in a comparison to free AChE. CNT/PAnNF film thicknesses could be preliminarily estimated by measuring UV absorbance of the dispersions (Abs. @ 350 nm), as illustrated in Fig. S8 B. The film thicknesses on a sensor were optimized based on the following factors: response time and response intensity, both of which are affected by diffusion in the nanocomposite film. To determine the optimal amount of CNT/PAnNF, nanosensors with the same amount of AChE, but different dilution of CNT/PAnNF stock were tested with 10 μL of 3 mM ACh and the results are shown in Fig. S9. It can be seen from this figure that the response of the nanosensors increases with increasing thickness of CNT/PAnNF and plateaus at 10-fold dilution (Abs. 0.65). Moreover, it was found that the response at 5-fold dilution starts slower, which is ascribed to too thick of a film. Therefore, the CNT/PAnNF dispersion providing an absorbance of 0.65 at 350 nm was selected for future studies, due to its steady dedoping rate, fast response time, and high intensity.

After selecting the optimal film parameters, a protective layer was coated on the AChE/CNT/PAnNF to form a sandwich-like structure to protect enzyme from leakage and improve AChE stability on the surface. Two types of protective layers, i.e., chitosan and polyethylene glycol (PEG), were evaluated. Chitosan and PEG are widely used, bio-friendly matrices for protection and entrapment of enzymes due to their biocompatibility, non-toxicity, abundance of functional groups, and resistance to chemical degradation. Under optimized conditions, PEG/AChE/CNT/PAnNF and Chitosan/AChE/CNT/PAnNF-modified electrodes were tested with different concentrations of AChE (Fig. 3A). Responses of both modified electrodes increase with increasing amounts of AChE. However, it was observed that Chitosan/AChE/CNT/PAnNF (Fig. 3A–a) outperformed PEG/AChE/CNT/PAnNF (Fig. 3A-b) at all AChE activity levels. These results indicate that chitosan is a more protective/

stable immobilization matrix than PEG (Kumar et al., 2020). Therefore, chitosan was selected as the protective layer for physical entrapment of AChE enzyme. Furthermore, using the results outlined in Fig. 3A-a, 0.13 U AChE was selected as the ideal enzyme concentration for preparing AChE-modified nanosensors.

Given that biosensor performance is affected by diffusion of ACh to immobilized AChE and PAnNF dedoping rate, both were considered for optimization of chitosan thickness. If chitosan film is too thick, enzyme will be fully protected with enhanced stability; however, diffusion of ACh and dedoping rate will be limited in the film. On the other hand, too thin chitosan film may not effectively protect AChE from leakage. As shown in Fig. 3B, the response of the Chitosan/AChE/CNT/PAnNF modified nanosensor is inversely proportional to the chitosan thickness. Thus, the results illustrate the limitations of thick films for ACh diffusion to immobilized AChE. The film prepared at 0.05% chitosan showed an ideal response. Therefore, 0.05% chitosan was selected for preparing the protection layer to protect AChE from leaking and retain enzyme activity.

Under optimal conditions, ACh was optimized using Chitosan/AChE/CNT/PAnNF nanosensors with 10 μL different concentrations of ACh ranging from 0.5 mM to 10 mM dried on a GF pad (2.5 mm diameter). As shown in Fig. 3C, biosensor response is linearly increased with ACh concentration and starts to level-off at ~3 mM ACh. Therefore, 3 mM ACh was selected for all experiments with the nanosensor in the forthcoming sections.

Finally, sample incubation time which allows OP to inhibit AChE was optimized. A standard solution of 15 μL 1 ppm Paraoxon-Methyl (PM) was tested with the biosensor at incubation periods of 1, 5, 10, 15, and 20 min (Fig. 3D). As seen in Fig. 3D, AChE inhibition by OP is increased with the increase of the sample incubation time and levels off at 10 min. Therefore, 10 min of sample incubation time was selected for determining the analytical performance and for in-vitro spiked food/environmental water samples.

3.5. Interference effects

Matrix effects significantly impact biosensor performance when testing real samples and is one of the biggest hurdles that any biosensor must overcome for real-world applications. There are two major categories of interferences from sample matrix for this biosensor: (i) AChE inhibitors besides pesticides in a sample; (ii) sample pH which affects both the catalytic activity of AChE and the transport properties of PAnNF. The sample pH is resulted from co-existing compounds, that may affect the transport properties of PAnNF and/or AChE activity.

Heavy metals, such as mercury (Hg), magnesium (Mg), lead (Pb), and copper (Cu), are commonly found in food/water samples, and have been reported to inhibit AChE activity (Rani et al., 2017; Shukor et al., 2013). To confirm metal-induced inhibitory effects of AChE, biosensors were tested with 1.0 μM Cu, Hg, and Pb. It was confirmed that AChE enzyme is inhibited by heavy metal ions and resulted in 24–31% inhibition for the measured concentrations (Table 1). To eliminate the effects of heavy metal ions on the performance of the AChE-based resistive nanosensor, EDTA was employed to bind free metal ions during the incubation period and prevent their inhibitory effects on AChE (Stepurska et al., 2015;

Tomlinson et al., 1981). It was found that AChE inhibition by heavy metal ions at 1.0 μM could be completely prevented in the presence of 1 mM EDTA (Table 1). We also found that EDTA had no effect on biosensor response without the presence of heavy metals. As such, 1 mM EDTA preloaded in the GF pre-treatment pad was used for real sample testing.

It has been well documented that pH affects the transport properties of PAnNFs and the catalytic activity of AChE (Vidal et al., 1982). The effect of pH on AChE activity was investigated and is maximized at pH 8 (Fig. S10), which is in accordance with prior works (Bergmann et al., 1956; Eränkö, 1972). As synthesized PAnNFs are partially-doped and are susceptible to changes in pH due to abundance of hydroxyl anions (OH^-) and hydrogen ions (H^+). Abundance of either OH^- or H^+ results in stripping or binding of protons within the PAnNF network, resulting in excessive dedoping or doping, respectively. To circumvent the effects of pH on AChE catalytic activity and PAnNF doping extent, samples were diluted 10 times to reduce the concentration of anions and ions within a sample (Stahnke et al., 2012). Furthermore, the use of dilution significantly decreases the concentration of other potential interferants, such as amino acids and glucose. To further reduce pH-related interference, GF pads were loaded with citric acid or sodium hydroxide to neutralize the pH, dependent on the sample type.

Finally, to further minimize the effect of co-existing compounds in a sample, samples are removed from the sensor surface after the sample incubation with a pre-treatment pad containing anti-interference reagents, as described in section 2.4. As such, interferants from a sample are removed prior to the addition of water and substrate for signal generation. In this case, the sensing signal is solely ascribed to the enzymatic reaction, not any related co-existing components. To confirm the validity of these approaches, we examined the responses of the nanosensors to 10-fold diluted food samples including grape juice, orange juice, milk, and beef without pesticides and found that these responses are comparable to the response to DI water (a control) with the average RSD of 5.8%. Therefore, the combination of sample dilution, sample pretreatment with pads containing anti-interference reagents, and removal of the sample prior to signal generation by enzyme reactions on a sensor was capable of mitigating interferences from sample matrices on the transport properties of PAnNFs and AChE activity.

3.6. Temperature effects

It is well known that temperature can improve catalytic activity of enzymes. However, temperatures exceeding 40 °C results in a decline in AChE activity (Gorne-Tschelnokow et al., 1993; Vidal et al., 1982). The effect of temperature on AChE activity and the interactions between OP and AChE were investigated at 5, 20, and 35 °C, with a sample containing paraoxon-methyl (PM) and a sample without PM (a control) (Fig. S11). Under the optimal conditions, AChE inhibition from controls positively correlate with temperature due to an increase in kinetic energy of the substrate to the enzyme, as expected. Furthermore, it was found that increasing the temperature during sample incubation containing different concentrations of PM resulted in increased AChE inhibition on the sensor surface, as well. This relationship is attributed to increased kinetic energy of PM to the active site of AChE. The observed linear dependence of AChE inhibition with temperature demonstrates potential

for compensating temperature effects for the biosensor, thus allowing for highly accurate on-site measurements of OP pesticides in food and environmental water.

3.7. Analytical performance of the biosensor

Under optimal conditions, the analytical performance of the resistive nanosensor was evaluated using PM as a model analyte. The nanosensor was tested with concentrations of PM ranging from 0.001 to 100 ppb. A sample without PM served as a control. AChE inhibition of the nanosensor was determined according to equation (1). The linear relationship of enzyme inhibition vs. the logarithm of the tested concentrations are illustrated in Fig. 4. The nanosensor exhibits a wide dynamic linear range from 0.001 to 100 ppb PM ($Y = 7.8782\ log_{10}\ (C_{PM}) + 38.15$, R = 0.9916) and a limit of detection (LOD) of ~0.304 ppt PM, using the 3 σ approach based on the relative standard deviation (RSD). The reproducibility of the nanosensor was further evaluated by measuring six replicates of each tested sample and was highly reproducible with RSD <5% for all concentrations. The total analysis time for each measurement is approximately 15 min, including the sample incubation period. Analytical performance of this biosensor was compared to those of biosensors recently published in literature (Table S12) and it was found that this work showed comparable or even superior analytical performance (Gai et al., 2023; Li et al., 2023; Yu et al., 2022; Zhu et al., 2020). Namely, the biosensor developed herein can detect pesticide residues as low as 1 ppt, comparable to those of recently published biosensing works.

To further evaluate the performance of the biosensor, the enzyme stability was evaluated with Chitosan/AChE/PAnNF/CNT nanosensors for 1 month (Fig. S13). During each week, the initial resistance of a biosensor was measured in its dry state and then the response of a biosensor (within the same batch) was measured with water and a signal generation pad. Results demonstrated that enzyme activity of biosensors fabricated from the same batch remained consistent from weeks 1–4. These results show the potential for long-term stability of the biosensor for 3–6 months.

3.8. Evaluation of the biosensor with in-vitro pesticide-spiked food and water samples

To explore the validity of the resistive nanosensor platform for field application; the biosensor was evaluated with 50 ppb PM-spiked food and environmental water samples (S4), including orange juice, grape juice, milk, ground beef, river and well water. To reduce matrix effects, samples were diluted 10-fold with DI water before analysis. Furthermore, orange and grape samples (pH ~ 3.5) were treated with pretreatment pads containing both 0.1 M NaOH to neutralize sample pH to ~7 and 1 mM EDTA. While, water samples were treated with pretreatment pads only containing EDTA to remove the possible presence of heavy metal ions.

Food/water samples without the addition of PM served as the control. The nanosensor was incubated with 15 μL of a 10-fold diluted sample for 10 min and then the sample was removed and the response of the nanosensor was recorded after adding 15 μL of water and a signal generation pad. The enzyme inhibition was determined based on equation (1) and the pesticide concentration was evaluated according to the calibration curve presented in

Fig. 4. To evaluate the reproducibility for real sample analysis, six replicates of each sample were measured. The results of food and environmental water testing are provided in Table 2. The recovery rate for real sample analysis ranged from 90–112% with an average of 98.3% for all 36 samples. Furthermore, the average reproducibility of the nanosensor was ~11.7% RSD for real samples. In parallel, the PM-spiked food and environmental water samples and their controls were analyzed by liquid chromatography-mass spectrometry (LC-MS), and the results are provided in Table 2. It was found that the results from this nanosensor, for all these samples, were in agreement with those from the standard LC-MS. Moreover, these results from this nanosensor demonstrate comparable and, in some cases, superior performance to those recently published biosensors in terms of recovery rate (S12). Furthermore, a more comprehensive set of food samples were evaluated in a comparison with LC-MS. As such, this nanosensor platform shows promise for rapid, sensitive, and quantitative detection of pesticides in food and environmental water.

4. Conclusion

In this work, we developed and evaluated an integrated smartphone/resistive enzymatic nanosensor for the detection of OP pesticides in food and water. The biosensor is portable and a sample to answer device that integrates all necessary reagents into the sensing platform, avoiding solution handling for onsite testing. Moreover, a mobile app provides a convenient tool for analyzing, displaying, and sharing testing results. Under optimal conditions, the resistive biosensor demonstrated a wide linear range (1 ppt–100 ppb), low LOD (0.304 ppt), short analytical time (~15 min), and high reproducibility (RSD <5%) for the detection of the model analyte, PM. Furthermore, the nanosensor was validated against LC-MS for PM-spiked food and environmental water samples, providing comparable results. As such, the integrated resistive biosensor platform shows promise as a field-deployable tool for pesticide analysis in food and water. Next, we will continue to develop the technology including long-term AChE stability (>6 months), additional food sample testing, and further investigation on reducing interference effects to ensure the capability of this biosensor in real world.

Supplementary Material

Refer to Web version on PubMed Central for supplementary material.

Acknowledgements

This work was financially supported by USDA SBIR award (2017-33610-26657) and NIH/NIEHS STTR award (1R41ES032388-01A1).

Data availability

No data was used for the research described in the article.

References

Anna S, 2016. Food Anal. Methods v 9 (6), 1654–1665-2016 v.1659 no.1656.

Arkhypova VN, Dzyadevych SV, Soldatkin AP, El'skaya AV, Jaffrezic-Renault N, Jaffrezic H, Martelet C, 2001. Talanta 55 (5), 919–927. [PubMed: 18968442]

Beltran J, López FJ, Hernández F, 2000. J. Chromatogr. A 885 (1–2), 389–404 [PubMed: 10941686]

Bergmann F, Segal R, Shimoni A, Wurzel M, 1956. Biochem. J 63 (4), 684–690. [PubMed: 13355871]

Berijani S, Assadi Y, Anbia M, Milani Hosseini M-R, Aghaee E, 2006. J. Chromatogr. A 1123 (1), 1–9. [PubMed: 16716329]

Dwevedi A, 2016. Basics of Enzyme Immobilization, Enzyme Immobilization, pp. 21–44.

Dzyadevych SV, Arkhypova VN, Martelet C, Jaffrezic-Renault N, Chovelon J-M, El'skaya AV, Soldatkin AP, 2004. Electroanalysis 16 (22), 1873–1882.

Dzyadevych SV, Soldatkin AP, Arkhypova VN, El'skaya AV, Chovelon J-M, Georgiou CA, Martelet C, Jaffrezic-Renault N, 2005. Sensor. Actuator. B Chem 105 (1), 81–87.

Eränkö L, 1972. Histochemie 33 (1), 1–14.

Gai P, Pu L, Wang C, Zhu D, Li F, 2023. Biosens. Bioelectron 220, 114841 [PubMed: 36323162]

Ghindilis AL, Morzunova TG, Barmin AV, Kurochkin IN, 1996. Biosens. Bioelectron 11 (9), 873–880. [PubMed: 8688164]

Godovsky DY, Varfolomeev AE, Zaretsky DF, Nayana Chandrakanthi RL, Kündig A, Weder C, Caseri W, 2001. J. Mater. Chem 11 (10), 2465–2469.

Gorne-Tschelnokow U, Naumann D, Weise C, Hucho F, 1993. Eur. J. Biochem 213 (3), 1235–1242. [PubMed: 8389298]

Hertz-Picciotto I, Sass JB, Engel S, Bennett DH, Bradman A, Eskenazi B, Lanphear B, Whyatt R, 2018. PLoS Med. 15 (10), e1002671. [PubMed: 30356230]

Huang J, Virji S, Weiller BH, Kaner RB, 2003. J. Am. Chem. Soc 125 (2), 314–315. [PubMed: 12517126]

Huang W-S, Humphrey BD, MacDiarmid AG, 1986. Journal of the chemical society. Faraday Trans. 1: Phys. Chem. Condensed Phases 82 (8), 2385–2400.

Karami-Mohajeri S, Abdollahi M, 2011. Hum. Exp. Toxicol 30 (9), 1119–1140. [PubMed: 21071550]

Kaur J, Singh PK, 2020. Phys. Chem. Chem. Phys 22 (27), 15105–15119. [PubMed: 32613964]

King AM, Aaron CK, 2015. Emerg. Med. Clin 33 (1), 133–151.

Kumar S, Gallagher R, Bishop J, Kline E, Buser J, Lafleur L, Shah K, Lutz B, Yager P, 2020. Analyst 145 (21), 6875–6886. [PubMed: 32820749]

Li H, Zhao S, Wang Z, Li F, 2023. Small 19 (14), 2206465.

Liang X, Han L, 2020. Adv. Funct. Mater 30 (28).

Liu G, Lin Y, 2005. Anal. Chem 77 (18), 5894–5901. [PubMed: 16159119]

Loguercio LF, Thesing A, Demingos P, de Albuquerque CD, Rodrigues RS, Brolo AG, Santos JF, 2021. Sensor. Actuator. B Chem 339, 129875.

Martini E, Merola G, Tomassetti M, Campanella L, 2015. Food Chem. 169, 358–365. [PubMed: 25236238]

Ozturk G, Alp S, Timur S, 2007. J. Mol. Catal. B Enzym 47 (3), 111–116.

Pundir CS, Chauhan N, 2012. Anal. Biochem 429 (1), 19–31. [PubMed: 22759777]

Rani S, Gupta RK, Yadav J, 2017. J. Entomol. Zool. Stud 5, 818–821.

Rezaee M, Assadi Y, Milani Hosseini M-R, Aghaee E, Ahmadi F, Berijani S, 2006. J. Chromatogr. A 1116 (1–2), 1–9. [PubMed: 16574135]

Shukor MY, Tham LG, Halmi MIE, Khalid I, Begum G, Syed MA, 2013. J. Environ. Biol 34 (5), 967–970. [PubMed: 24558814]

Souza Tette PA, Rocha Guidi L, de Abreu Glória MB, Fernandes C, 2016. Talanta 149, 124–141. [PubMed: 26717823]

Stahnke H, Kitdaus S, Kempe G, Alder L, 2012. Anal. Chem 84 (3), 1474–1482. [PubMed: 22243135]

Stejskal J, Kratochvíl P, Radhakrishnan N, 1993. Synth. Met 61 (3), 225–231.

Stepurska KV, Soldatkin CO, Kucherenko IS, Arkhypova VM, Dzyadevych SV, Soldatkin AP, 2015. Anal. Chim. Acta 854, 161–168. [PubMed: 25479880]

Thakkar JB, Gupta S, Prabha CR, 2019. Int. J. Biol. Macromol 137, 895–903. [PubMed: 31247229]

Tomlinson G, Mutus B, McLennan I, 1981. Can. J. Biochem 59 (9), 728–735. [PubMed: 7317819]

Vidal CJ, MuÑOz E, Gómez-FernÁNdez JC, Lozano JA, 1982. Biochem. Soc. Trans 10 (5), 374–375.

Virji S, Huang J, Kaner RB, Weiller BH, 2004. Nano Lett. 4 (3), 491–496.

Wang J, Timchalk C, Lin Y, 2008. Environ. Sci. Technol 42 (7), 2688–2693. [PubMed: 18505017]

Yu G, Wu W, Zhao Q, Wei X, Lu Q, 2015. Biosens. Bioelectron 68, 288–294. [PubMed: 25594160]

Yu L, Chang J, Zhuang X, Li H, Hou T, Li F, 2022. Anal. Chem 94 (8), 3669–3676. [PubMed: 35166114]

Zhang Y, Hei T, Cai Y, Gao Q, Zhang Q, 2012. Anal. Chem 84 (6), 2830–2836. [PubMed: 22339669]

Zhu D, Zhang M, Pu L, Gai P, Li F, 2022. Small 18 (3), 2104993.

Zhu Y, Wu J, Han L, Wang X, Li W, Guo H, Wei H, 2020. Anal. Chem 92 (11), 7444–7452. [PubMed: 32363854]

Zou Z, Du D, Wang J, Smith JN, Timchalk C, Li Y, Lin Y, 2010. Anal. Chem 82 (12), 5125–5133. [PubMed: 20507134]

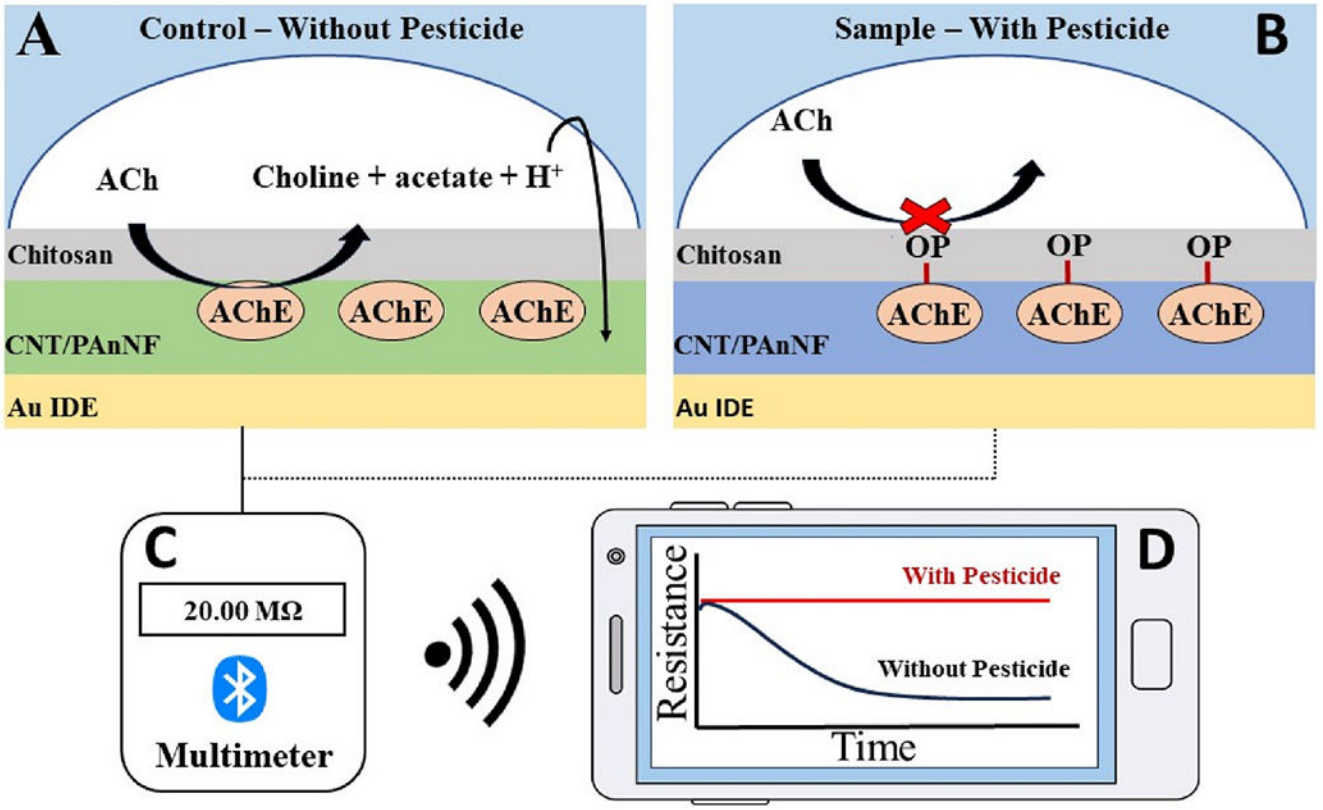

Fig. 1.

Schematic of Chitosan/AChE/CNT/PAnNF biosensor for detection of OP pesticides in food and water. **(A)** Without OP pesticides, the biosensor can produce a large resistance decrease due to AChE generating a large number of protons, doping the PAnNFs. **(B)** With OP pesticides, the biosensor produces a reduced resistance decrease, due to less proton generation because of AChE inhibition by OP pesticides. **(C)** A multimeter with Bluetooth acquires resistance data from a biosensor and transfers the data to a smartphone. **(D)** With the app, smartphone displays the resistance changes resulted from a sample, e.g., a control sample (black line), and a sample with pesticide (red line). (For interpretation of the references to color in this figure legend, the reader is referred to the Web version of this article.)

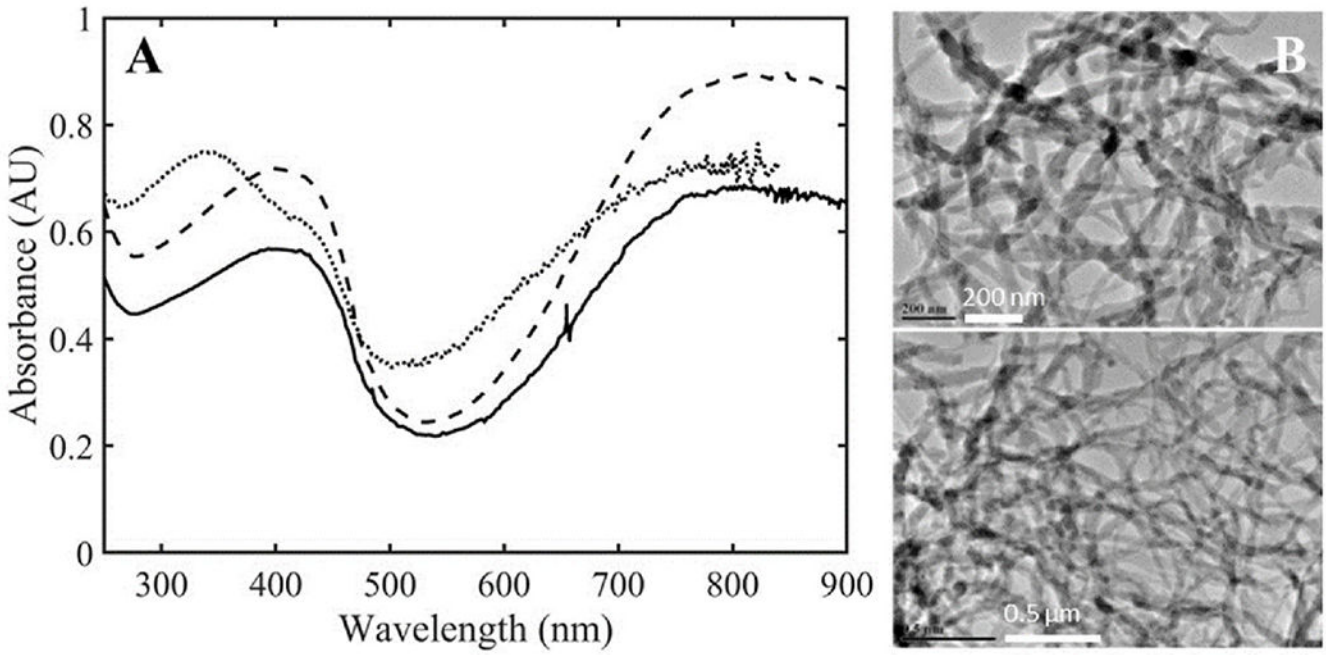

Fig. 2.

Characterization of CNT/PAnNF nanocomposites. **(A)** UV–Vis spectra of HCl fully-doped PAnNF with wt. 0% CNT (dashed) and 1.0% CNT (solid) and partially-doped PAnNF/CNT with wt. 1.0% CNT (dotted line) **(B)** Transmission electron microscopy images of CNT/PAnNF nanocomposites with (top) 0% CNT and (bottom) 1% CNT.

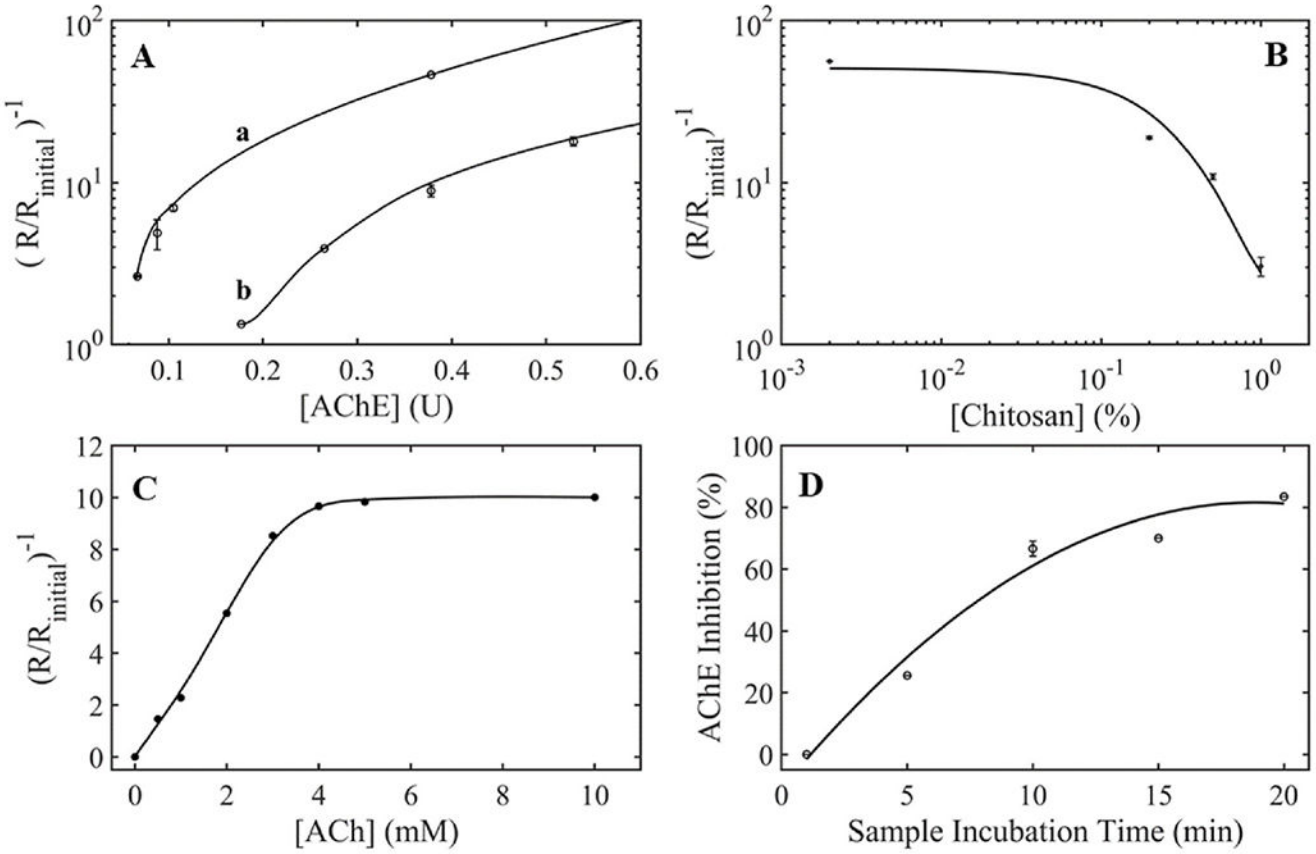

Fig. 3.

Optimization of the biosensor with different parameters. **[A]** Response of biosensors to: **(a)** 0.05% chitosan, and **(b)** 0.05% PEG as a protection layer under different concentrations of AChE (U): **(a)** 0.067, 0.088, 0.11, and 0.38 **(b)** 0.18, 0.26, 0.38, and 0.53. **[B]** Response of biosensors to different amounts of chitosan: 0.002%, 0.2% 0.5%, and 1% on the surface of the AChE/CNT/PAnNF film. 0.13 U AChE and 10 μL 3 mM Ach were used for each testing. **[C]** Response of biosensors to different concentrations of ACh loaded on a GF pad: 0, 0.5, 1, 2, 3, 4, 5, and 10 mM. 0.13 U AChE and 0.02% chitosan were used. **[D]** The curve of enzyme inhibition vs. different sample incubation time with optimal biosensors: 1, 5, 10, 15, and 20 min. Samples containing 15 μL 1 ppm Paraoxon-Methyl was used here.

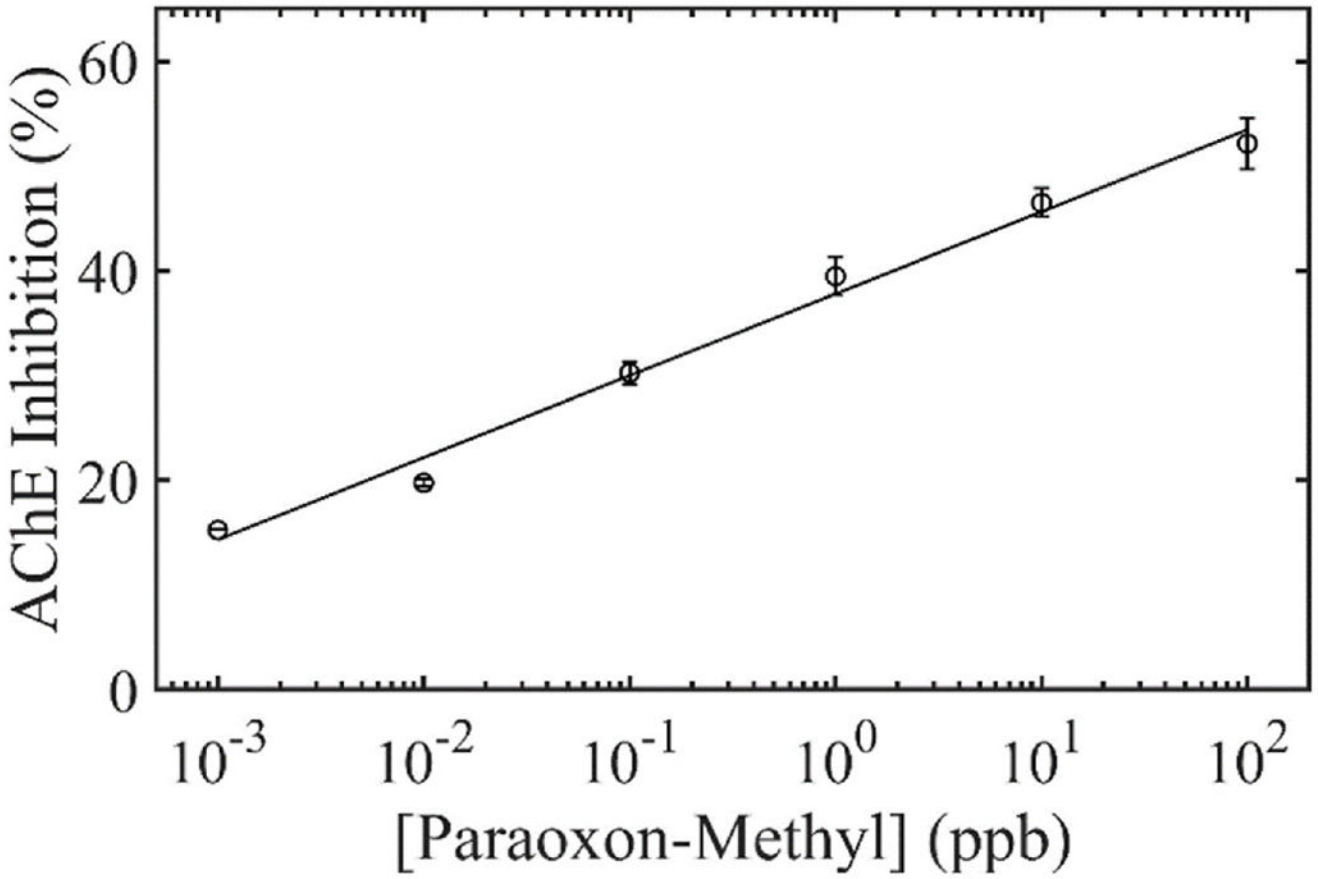

Fig. 4.

Calibration curve of the biosensor for Paraoxon-Methyl at concentrations of 100, 10, 1, 0.1, 0.01, and 0.001 ppb under optimal conditions: a 2 μL 0.05% chitosan and 2 μL 0.13 U AChE in 1 mM PBS, on a CNT/PAnNF film (Absorbance 0.65 @ 350 nm). Response generated using 10 μL 3 mM ACh pre-loaded on a GF pad.

Table 1

Analyzing a sample containing heavy metal using biosensor with and without 10.0 mM EDTA.

Sample	AChE Inhibition$_{\text{without EDTA}}$ (%)	AChE Inhibition$_{\text{with EDTA}}$ (%)
Mercury	28.76	0
Copper	31.09	0
Lead	24.38	0

Note: Samples contain Hg^{2+}, Cu^{2+}, or Pb^{2+} at a concentration of 1.0 μM.

Table 2

Comparative results between biosensor and mass spectrometry for analysis of 50 ppb PM-spiked river water, well water, orange juice, grape juice, milk, and beef.

Sample	Paraoxon-Methyl (ppb)	Nanosensor (ppb)	Recovery (%)	RSD (%)	LC-MS (ppb)	Recovery (%)
Orange Juice	50	55.9 ± 6.1	111.8	10.82	59.7 ± 1.15	106.6
Grape Juice	50	44.9 ± 4.16	90	9.27	66.5 ± 4.10	132.9
Milk	50	48.2 ± 6.26	96.5	12.99	53.7 ± 6.66	107.3
Ground Beef	50	46.7 ± 6.01	93.5	12.87	33.7 ± 2.91	67.5
River Water	50	47.6 ± 6.6	95.2	13.80	53.7 ± 0.71	106.6
Ground Water	50	50.6 ± 5.27	101	10.42	61.2 ± 1.00	122.4